Journal of Medicinal Chemistry Article

J. Med. Chem. **2010,** *53,* 5587–5596 **5587**
DOI: 10.1021/jm100261r

Lysine N^{ϵ}-Trimethylation, a Tool for Improving the Selectivity of Antimicrobial Peptides

María Fernández-Reyes,[†] Dolores Díaz,[†] Beatriz G. de la Torre,[‡] Ania Cabrales-Rico,[‡,§] Mariona Vallès-Miret,[‡,∥] Jesús Jiménez-Barbero,[†] David Andreu,*[,‡] and Luis Rivas*[,†]

[†]*Centro de Investigaciones Biológicas CSIC, Ramiro de Maeztu 9, 28040 Madrid, Spain, and* [‡]*Departament de Ciències Experimentals i de la Salut, Universitat Pompeu Fabra, Dr. Aiguader 88, 08003 Barcelona, Spain.* [§]*Present address: Centro de Ingeniería Genética y Biotecnología, La Habana, Cuba.* [∥]*Present address: School of Chemistry, University of Edinburgh, Edinburgh EH9 3JJ, U.K.*

Received March 1, 2010

The effects of lysine N^{ϵ}-trimethylation at selected positions of the antimicrobial cecropin A−melittin hybrid peptide KWKLFKKIGAVLKVL-amide have been studied. All five monotrimethylated, four bis-trimethylated plus the per-trimethylated analogues have been synthesized and tested for antimicrobial activity on *Leishmania* parasites and on Gram-positive and -negative bacteria, as well as for hemolysis of sheep erythrocytes as a measure of cytotoxicity. The impact of trimethylation on the solution conformation of selected analogues has been evaluated by NMR, which indicates a slight decrease in the α-helical content of the modified peptides, particularly in the N-terminal region. Trimethylation also enhances the proteolytic stability of mono- and bis-trimethylated analogues by 2−3-fold. Although it tends to lower antimicrobial activity in absolute terms, trimethylation causes an even higher decrease in hemolytic activity and therefore results in improved selectivity for several analogues. The monotrimethylated analogue at position 6 shows the overall best selectivity against both the *Leishmania donovani* protozoan and *Acinetobacter baumannii*, a Gram-negative bacterium of increasing clinical concern.

Introduction

Eukaryotic antimicrobial peptides (AMPs[a]), either present or induced in a host after initial contact with a pathogen,[1] pose a first chemical barrier against infection.[2] Pathogen recognition by AMPs involves molecular traits common to a wide variety of microorganisms. For instance, anionic phospholipids exposed at the outer leaflet of the plasma membrane underscore AMP specificity for prokaryotes and lower eukaryotes, because in higher eukaryotes, these phospholipids are confined to the cytoplasmic face of the membrane.[3] The strong cationic nature of most AMPs, plus their tendency to adopt amphipathic conformations, favors accumulation and insertion into the pathogen membrane, leading to its disruption or to AMP translocation and eventual damage to intracellular structures.[4] In either case, development of resistance is less likely than for other antimicrobials, involving as it would major changes in phospholipid composition and architecture, in turn requiring substantial overhauling of membrane-based enzymatic and transport systems.[5]

While AMPs have raised expectations as alternatives to conventional antibiotics in the face of a worldwide increase in pathogen multiresistance[6] and of a relatively exhausted pipeline of antimicrobial leads, they still have to gain a foothold in therapeutics, largely due to limitations intrinsic to their peptide nature such as short in vivo half-lives, or side-effects unrelated to antimicrobial activity,[7] all of them requiring careful optimization before clinical assays can be implemented.[1,8]

Residue-specific modification of bioactive peptides is one of the most effective and broadly used strategies for peptide lead optimization.[9] For a significant number of small and even medium-sized bioactive peptides, including quite a few AMPs, both the size and the scarcity of complex posttranslational modifications (i.e., disulfide bridges) underpin the synthesis-based strategies and have thus resulted in a wealth of analogues incorporating modifications such as non-natural residues, site-specific epimerization, acylation, glycosylation, or mobility restriction (e.g., by internal disulfide, helix stapling, etc.) aimed at preserving privileged conformational features[10−12]

The ε-amino group of Lys has been frequently used for conjugation to other biomolecules (fatty acids, nucleic acids) or drugs, or for cross-linking to other proteins or peptides. It has also recently received attention for its in vivo role in a vast variety of modifications, e.g., methylation, acetylation, ubiquitination, sumoylation, or citrullination (reviewed in ref 13),

*To whom correspondence should be addressed. For D.A.: phone, +34-933160868; fax, +34-933160901; e-mail, david.andreu@upf.edu. For L.R.: phone, +34-918373112; fax, +34-915360432; e-mail, luis.rivas@cib.csic.es.

[a]Abbreviations: AMP, antimicrobial peptide; ATCC, American Type Culture Collection; Boc, *tert*-butoxycarbonyl; CA, cecropin A; CA-M, cecropin A-melittin hybrid peptide; CECT, Spanish Type Culture Collection; COSY, correlated spectroscopy; DIEA, *N*,*N*-diisopropylethylamine; DMF, *N*,*N*-dimethylformamide; Fmoc, 9-fluorenylmethyloxycarbonyl; HBTU, 2-(1*H*-benzotriazole-1-yl)-1,1,3,3-tetramethyluronium hexafluorophosphate; HC_{50}, peptide concentration causing 50% hemoglobin release; HOBt, *N*-hydroxybenzotriazole; HPLC, high performance liquid chromatography; IC_{50}, peptide concentration causing 50% inhibition of MTT reduction at 4 h incubation; LC-MS, liquid chromatography coupled to mass spectrometry; LC_{50}, peptide concentration causing 50% inhibition of *Leishmania* proliferation; M, melittin; MALDI-TOF, matrix-assisted laser desorption ionization, time-of-flight analysis; MIC_{50}, peptide concentration causing 50% inhibition of bacterial growth; MS, mass spectrometry; MTT, 3-(4,5-dimethylthiazol-2-yl)-2,5-diphenyltetrazolium bromide; NOESY, nuclear Overhauser enhancement spectroscopy; rmsd, root-mean-square deviation; SI, selectivity index (= HC_{50}/LC_{50} or HC_{50}/MIC_{50}); TFA, trifluoroacetic acid; TOCSY, total correlated spectroscopy; TSP, 2,2,3,3-tetradeutero-3-trimethylsilylpropionic acid.

Published on Web 07/09/2010

Table 1. Structures and Chemical Characterization of CA(1−7)M(2−9) and Trimethyl-Lys Analogues

peptide	sequence/replacement	sequence[a]	t_R (min)[b]	mass expected	mass found[c]
1	CA(1−7)M(2−9)	KWKLFKKIGAVLKVL	9.53	1769.18	1770
2	K_1 (Me_3)	**K**WKLFKKIGAVLKVL	9.05	1812.24	1813
3	K_3 (Me_3)	KW**K**LFKKIGAVLKVL	9.11	1812.24	1813
4	K_6 (Me_3)	KWKLF**K**KIGAVLKVL	9.10	1812.24	1813
5	K_7 (Me_3)	KWKLFK**K**IGAVLKVL	9.24	1812.24	1813
6	K_{13} (Me_3)	KWKLFKKIGAVL**K**VL	9.22	1812.24	1813
7	$K_{1,3}$ $(Me_3)_2$	**K**W**K**LFKKIGAVLKVL	9.12	1855.29	1856
8	$K_{3,6}$ $(Me_3)_2$	KW**K**LF**K**KIGAVLKVL	9.03	1855.29	1856
9	$K_{6,7}$ $(Me_3)_2$	KWKLF**KK**IGAVLKVL	9.14	1855.29	1856
10	$K_{1,13}$ $(Me_3)_2$	**K**WKLFKKIGAVL**K**VL	9.19	1855.29	1856
11	$K_{1,3,6,7,13}$ $(Me_3)_5$	**K**W**K**LF**KK**IGAVL**K**VL	9.01	1984.45	1985

[a] All peptides in C-terminal carboxamide form. Lysine (K) residues in bold are trimethylated. [b] Linear 5−95% B into A gradient over 20 min. A = 0.1% formic acid in water; B = 0.08% formic acid in acetonitrile. For all peptides, HPLC purity was >95%. [c] Determined by LC-MS.

Table 2. Leishmanicidal and Hemolytic Activities of CA(1-7)M(2-9) and Its Trimethylated Derivatives

peptide	sequence/replacement	*L. donovani* promastigotes IC_{50} (μM)[a]	*L. donovani* promastigotes LC_{50} (μM)[a]	*L. donovani* promastigotes SI[b]	*L. pifanoi* amastigotes IC_{50} (μM)[a]	*L. pifanoi* amastigotes LC_{50} (μM)[a]	*L. pifanoi* amastigotes SI[b]	erythrocytes HC_{50} (μM)[a]
1	CA(1−7)M(2−9)	1.8 (±0.0)	1.5 (±0.1)	26.8 (1.0)	4.3 (±0.2)	4.5 (±0.2)	8.9 (1)	40.2 (±2.2)
2	K_1 (Me_3)	3.9 (±0.3)	2.8 (±0.0)	27.6 (1.0)	6.0 (±0.8)	6.4 (±1.2)	12.0 (1.3)	77.2 (±11.1)
3	K_3 (Me_3)	3.3 (±0.0)	3.1 (±0.6)	27.6 (1.0)	9.4 (±0.8)	8.2 (±1.0)	10.4 (1.2)	85.6 (±4.6)
4	K_6 (Me_3)	3.7 (±0.0)	1.7 (±0.0)	92.7 (3.4)	13.4 (±0.1)	16.3 (±1.30)	9.6 (1.1)	157.6 (±7.3)
5	K_7 (Me_3)	3.7 (±0.2)	2.3 (±0.0)	71.3 (2.6)	11.4 (±0.8)	12.1 (±1.2)	13.5 (1.5)	164.0 (±7.8)
6	K_{13} (Me_3)	3.5 (±0.1)	2.5 (±0.0)	63.0 (2.3)	10.1 (±0.6)	11.6 (±0.5)	13.5 (1.5)	157.4 (±1.0)
7	$K_{1,3}$ $(Me_3)_2$	12.8 (±0.4)	15.5 (±0.6)	6.7 (0.2)	16.2 (±0.1)	24.8 (±1.2)	4.2 (0.5)	105.0 (±3.5)
8	$K_{3,6}$ $(Me_3)_2$	5.1 (±0.2)	6.7 (±0.2)	17.4 (0.6)	7.4 (±0.3)	16.5 (±1.6)	7.1 (0.8)	117.3 (±13.9)
9	$K_{6,7}$ $(Me_3)_2$	6.1 (±0.1)	5.3 (±0.6)	25.3 (0.9)	9.2 (±2.0)	27.0 (±1.2)	4.9 (0.5)	134.0 (±8.8)
10	$K_{1,13}$ $(Me_3)_2$	8.8 (±0.3)	7.6 (±0.1)	10.8 (0.4)	17 0.0(±3.0)	13.5 (±1.4)	6.1 (0.7)	82.6 (±12.4)
11	$K_{1,3,6,7,13}$ $(Me_3)_5$	>50	>50	nd	>50	>50	nd	>200

[a] In parentheses, standard deviation. [b] Selectivity index (SI) as defined in text; in parentheses, improvement in SI relative to parent peptide **1**.

of the histone proteins that regulate the transcriptional status of chromatin.[14−17] This interest in Lys side chain modification, particularly methylation, by the epigenetics community contrasts with the relative lack of references to Lys methylation in the AMP field, excepting (1) histone-related sequences with reported antimicrobial activities,[18−24] (2) a methylated analogue of the decapeptide KSL used in chewing gum,[25] (3) lactoferricin,[26] or (4) melittin, which entirely loses its hemolytic activity upon trimethylation of all its Lys residues.[27]

In this work, we have further investigated the effect of Lys trimethylation on antimicrobial activity and hemolysis (as a measure of cytotoxicity) of AMPs. To this end we have chosen a well-tested, simple AMP platform, namely the cecropin A−melittin (CA-M) hybrid CA(1−7)M(2−9), KWKLFKKIGAVLKVL-amide (reviewed in refs 28,29). In this peptide,[30,31] the N-terminal (first seven residues) cationic region of nonhemolytic cecropin A is fused to the more hydrophobic, also nonhemolytic N-terminus of melittin, the resulting hybrid structure showing an improvement in both antimicrobial and cytotoxic activities relative to the parent structures. CA(1−7)M(2−9) and some congeners have shown activity on a variety of microorganisms, including bacteria,[32−34] fungi,[35,36] or protozoa,[31,37−39] as well as in animal[33,40,41] and plant disease models.[36,42]

Predictable effects of Lys trimethylation include (1) retaining the same global charge, (2) increased bulkiness and hydrophobicity of the side chains, and (3) ε-amino groups (quaternary) with no hydrogen bonding ability. Our exploration of these aspects on the CA(1−7)M(2−9) model underpins Lys trimethylation as a useful tool for modulating antimicrobial activity and half-life, and restates the case for CA-M hybrids as potential antimicrobial candidates against multiresistant pathogens.

Results

Trimethylated Derivatives of CA(1−7)M(2−9). Structures of the parent peptide (**1**), all five singly trimethylated (**2**−**6**), plus four doubly trimethylated (**7**−**10**) and the fully trimethylated (**11**) analogues are shown in Table 1. All peptides were made by Fmoc solid phase synthesis methods,[43] using commercially available Fmoc-Lys(Me_3)-OH at the designated positions. After full deprotection and cleavage from the resin, peptides were purified to near-homogeneity (>95%) by preparative RP-HPLC and characterized by electrospray MS, as they showed poor desorption by MALDI-TOF. In selected cases (see below), additional characterization by NMR was done.

Activity against *Leishmania* and Erythrocytes. *Leishmania* was chosen as the model target microorganism for measuring antimicrobial activity due to its lack of tightly packed external barriers such as the outer membrane or peptidoglycan layer of Gram-negative and Gram-positive bacteria, respectively. For measuring hemolysis, sheep erythrocytes were selected. Activities of peptides **1**−**11** on the two forms (promastigote, amastigote) of the parasite and on erythrocytes are shown in Table 2.

A general trend observed was the gradual decrease in both antimicrobial and cytotoxic activity as the number of Lys-(Me_3) residues in the sequence increased. The nontrimethylated lead **1**, CA(1−7)M(2−9), was most active, while full trimethylation (analogue **11**) caused complete inhibition of all activities within the range of concentrations tested. Within this general trend, subtle variations could be observed.

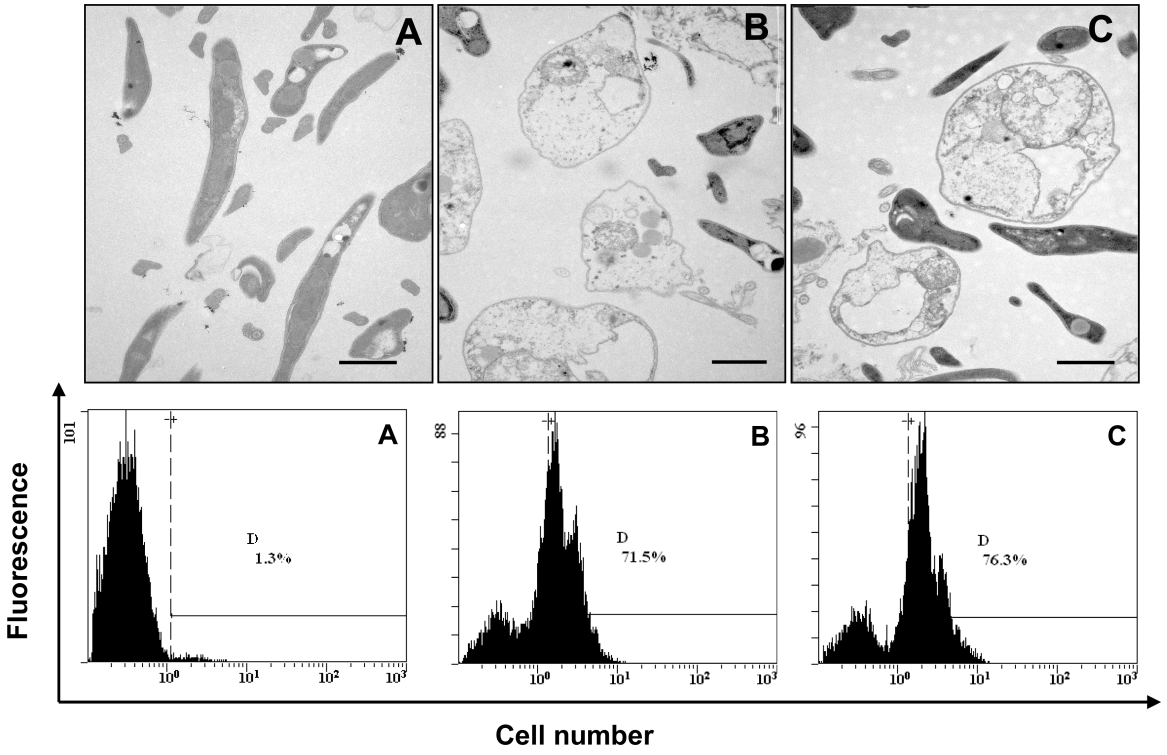

Figure 1. Morphological damage and distribution of trimethylated Lys peptides on *Leishmania*. Upper panels: Electron microscopy of *L. donovani* promastigotes ((A) control parasites; (B) treated with 4 μM CA(1−7)M(2−9) (**1**); (C) treated with 6 μM $K_7(Me_3)$ analogue (**5**) showing depletion of intracitoplasmic electron-dense material (bar = 1 μm). Lower panels: Cytofluorometric assay of the incorporation of Sytox Green under the same conditions assayed for electron microscopy. Percentage of cells incorporating the vital dye (peaks on the right) is indicated inside each panel.

For instance, for monosubstituted analogues tested on *Leishmania* promastigotes, antiparasitic activity was relatively independent of the location of the Lys(Me_3) residue, whereas in the disubstituted series, analogue **7**, with Lys(Me_3) replacements at the positions closest to the N-terminus, underwent the most significant activity loss. In amastigotes, although a similar trend was observed, differences between analogues were less clear. In the hemolysis assays, the drop in activity was particularly acute for three monosubstituted analogues (**4**−**6**) yet not so pronounced for the four doubly trimethylated peptides (**7**−**10**) tested.

Contrasting the cytotoxic and antiparasitic activities of each peptide by means of the selectivity index, (SI, defined as HC_{50}/LC_{50}, Table 2), it is clear that, for some analogues and particularly against the promastigote forms of *Leishmania*, the Lys(Me_3) replacement entails a substantial improvement in SI. Thus, for analogues **4**−**6**, 2−3-fold SI enhancements were found relative to parent peptide **1**, with antimicrobial activities still well into the low-micromolar range. For amastigotes, two of the above peptides (**5** and **6**) also displayed enhanced SIs, but to a lower extent. On the other hand, all of the four double Lys(Me_3) replacements investigated (analogues **7**−**10**) resulted in lower SIs.

An additional conclusion to be drawn from Table 2 is that the IC_{50}/LC_{50} ratio for most peptides on promastigotes is close to 1, which means that the peptide effect after the first 4 h incubation is basically irreversible. In contrast, for three of the doubly substituted analogues tested (**7**−**9**), the short-term inhibition (IC_{50}) of the peptides on amastigotes is more pronounced than the inhibition of proliferation (LC_{50}), suggesting that the amastigote has a substantial ability to recover from the initial blow.

Electron Microscopy. Electron microscopy provides useful insights into the morphological effects of peptides on microbes, and those may in turn provide useful clues on the lethal mechanism. The damage inflicted by the peptides to *Leishmania* promastigotes is illustrated in Figure 1. To avoid any bias due to the differential killing ability of the peptides, they were assayed at equipotent concentrations, i.e., equivalent to those inducing a 70% inhibition of MTT reduction. In all cases, and regardless of the peptide assayed, extensive permeabilization, with translucent cytoplasm and extensive damage to the plasma membrane, was observed. This pattern was followed by most, though not all, parasites in the same field, with some displaying an apparently undamaged plasma membrane and no evidence of leakage of cytoplasmic material.

Investigation of Lethal Mechanisms. In view of the electron microscopy data, and in accordance with previous studies on the mechanism of action of other CA-M peptides,[39,44] we explored the membrane permeation activity of Lys(Me_3)-substituted peptides on *Leishmania* promastigotes by two complementary methods: (1) enhanced fluorescence of the vital dye Sytox Green (MW = 600 Da), which binds exclusively the nucleic acids of permeabilized cells, and (2) membrane depolarization. As seen in Figure 2, all active peptides were able to induce the entrance of the dye into parasites in a dose-dependent manner, as illustrated for peptides **1**, **5**, and **10** on both promastigotes and amastigotes. For all of them, a rapid increase in Sytox Green fluorescence followed peptide addition, reaching a maximal value in less than 10 min.

Plasma membrane depolarization experiments furnished comparable results. An increase in fluorescence, irreversible

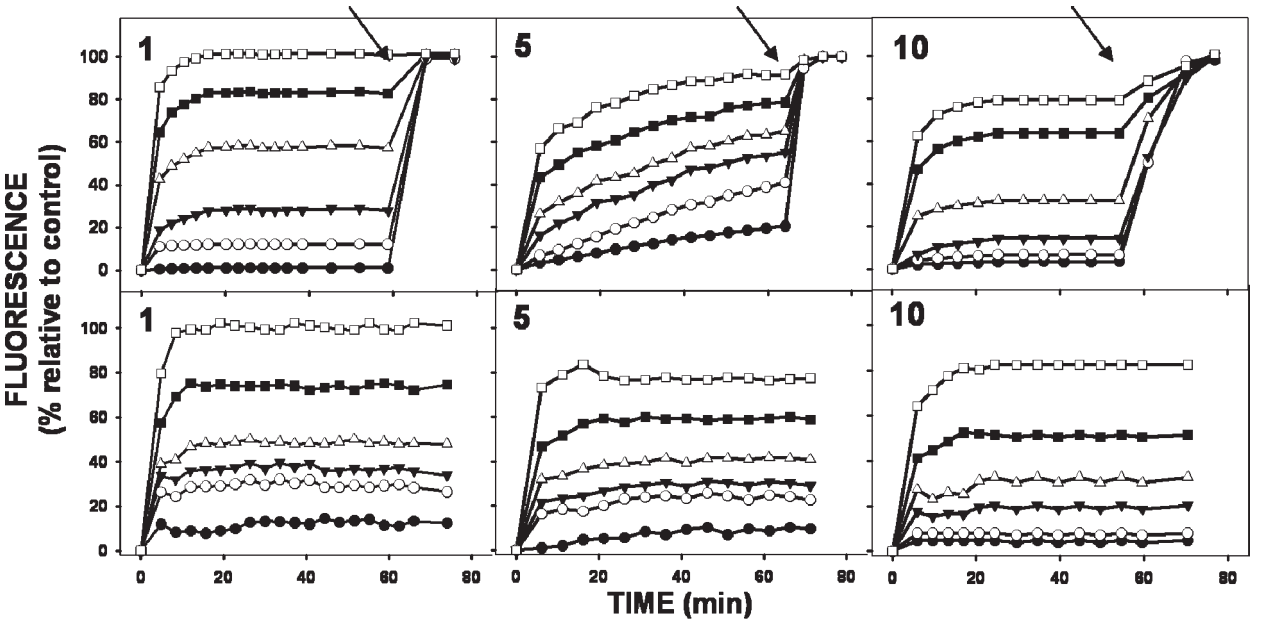

Figure 2. Permeation of *L. donovani* promastigote plasma membrane by peptides CA(1−7)M(2−9) (**1**), $K_7(Me_3)$ (**5**), and $K_{1,13}(Me_3)_2$ (**10**). Upper panels: kinetics of Sytox Green entrance after peptide addition ($t = 0$), measured by the increase in fluorescence after binding of the dye to intracellular nucleic acids ($\lambda_{exc} = 504$ nm; $\lambda_{ems} = 524$ nm). Full permeation (100%) is achieved after addition of 0.1% Triton X100 (indicated by arrow). Peptide concentrations (μM): 0.5 (●), 1.0 (○); 1.5 (▼); 2.0 (△); 4.0 (■); 6.0 (□). Lower panels: Promastigote plasma membrane depolarization measured by the increase in fluorescence of bisoxonol ($\lambda_{exc} = 540$ nm; $\lambda_{ems} = 580$ nm). Full depolarization was defined as that achieved by addition of 3 μM CA(1−8)M(1−18) (see ref 37).

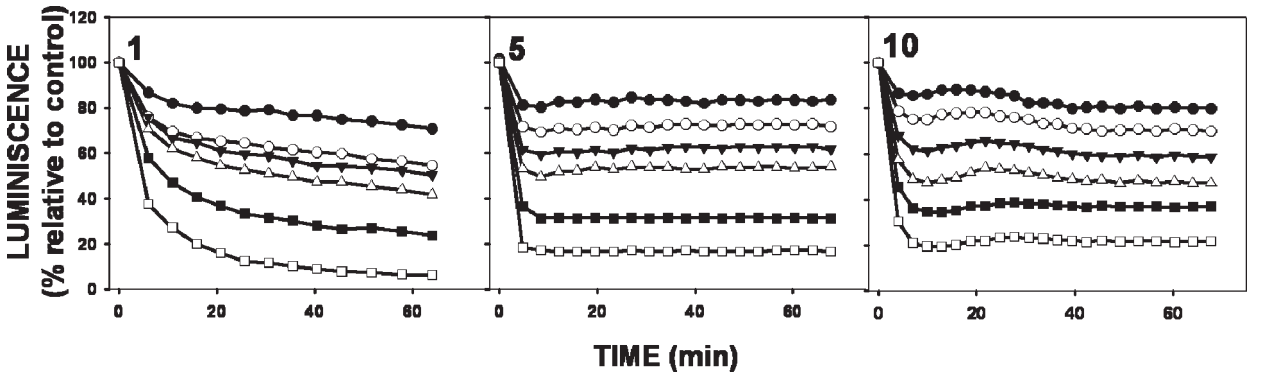

Figure 3. Real-time depletion of intracellular ATP levels upon peptide addition in living *L. donovani* 3-Luc promastigotes. See ref 39 for details. Peptide nomenclature and concentration as in Figure 2. Peptide added at $t = 0$ (luminescence = 100%). Luminiscence was corrected relative to control parasites.

over the entire observation period, was found (Figure 2, lower panels). Depolarization has the advantage over vital dye uptake experiments of its dynamic character, i.e., changes in bisoxonol fluorescence reflect dye insertion into the parasite plasma membrane, driven by the collapse of membrane potential, and hence are potentially reversible if the parasite recovers from its membrane lesions. In contrast, Sytox Green uptake relies on the high-affinity interaction of the dye with intracellular nucleic acids, a practically irreversible process impervious to any membrane-repairing effort after peptide insertion. In this particular case, however, both approaches yielded comparable results, indicating that the peptides caused irreversible damage to the membrane.

To account for the electron microscopy observation of apparently unharmed organisms at peptide concentrations that diminish parasite proliferation, the entrance of Sytox Green in individual cells was also assessed by cytofluorometry (Figure 1, lower panels). Two distinct cell populations were readily identified, a minor one, essentially unlabeled, and a major one (>70%), incorporating the dye, a situation suggesting an all-or-none effect of the peptides.

To illustrate the rapid physiological impairment of the parasite caused by the peptides, variations in the ATP pool were monitored. To this end, 3-Luc strain promastigotes expressing a cytoplasmic form of luciferase[39] were used in conjunction with caged-free permeable DMNPE-luciferin, a setting with ATP as the limiting factor for luminescence. As shown in Figure 3, all three analogues tested (**1**, **5**, **10**) caused a fast, dose-dependent drop in luminescence upon addition to the parasite suspension, confirming fast bioenergetic collapse upon peptide addition.

Bactericidal Activity of Trimethylated Analogues. Given the success of Lys trimethylation in improving the SI of CA(1−7)M(2−9) on *Leishmania*, it seemed appropriate to test also the activity of $Lys(Me_3)$-substituted peptides on bacteria. To this end, a representative Gram positive (*Staphylococcus aureus*) and an opportunistic Gram negative (*Acinetobacter baumannii*) were chosen as targets. Results are

Table 3. Bactericidal and Hemolytic Activities of CA(1−7)M(2−9) and Its Trimethylated Derivatives

		S. aureus		*A. baumannii*		erythrocytes
peptide	sequence/replacement	MIC_{50} (μM)[a]	SI[b]	MIC_{50} (μM)[a]	SI[b]	HC_{50} (μM)[a]
1	CA(1−7)M(2−9)	2.9 (±0.1)	13.8 (1.0)	1.1 (±0.3)	36.5 (1.0)	40.2 (±2.2)
2	K_1 (Me_3)	3.4 (±0.1)	22.7 (1.6)	1.3 (±0.1)	59.4 (1.7)	77.2 (±11.1)
3	K_3 (Me_3)	2.4 (±0.1)	35.7 (2.6)	1.7 (±0.3)	50.3 (1.4)	85.6 (±4.6)
4	K_6 (Me_3)	4.6 (±0.2)	34.3 (2.5)	1.4 (±0.1)	112.2 (3.0)	157.6 (±7.3)
5	K_7 (Me_3)	7.2 (±0.6)	22.8 (1.6)	1.9 (±0.4)	86.3 (2.3)	164.0 (±7.8)
6	K_{13} (Me_3)	4.4 (±0.2)	35.8 (2.6)	2.1 (±0.1)	74.9 (2.0)	157.4 (±1.0)
7	$K_{1,3}$ $(Me_3)_2$	8.0 (±0.0)	13.1 (0.9)	3.5 (±0.5)	30.0 (0.8)	105.0 (±3.5)
8	$K_{3,6}$ $(Me_3)_2$	6.2 (±0.5)	18.9 (1.4)	2.0 (±0.1)	58.6 (1.6)	117.3 (±13.9)
9	$K_{6,7}$ $(Me_3)_2$	10.7(±2.9)	12.5 (0.9)	2.6 (±0.1)	51.5 (1.4)	134.0 (±8.8)
10	$K_{1,13}$ $(Me_3)_2$	4.5 (±0.3)	18.4 (1.3)	1.8 (±0.5)	45.8 (1.25)	82.6 (±12.4)
11	$K_{1,3,6,7,13}$ $(Me_3)_5$	> 30	nd	> 30	nd	> 200

[a] In parentheses, standard deviation. [b] Selectivity index (SI) as defined in text; in parentheses, improvement in SI relative to parent peptide **1**.

shown in Table 3. For *S. aureus*, the activity tended to drop slightly as the level of Lys(Me_3) substitution increased, similar to *Leishmania*, although in this case the trend was less uniform (compare, e.g., disubstituted analogue **10** with monosubstituted **4** or **6**). For *A. baumannii*, a comparable behavior was seen, although the range of variation was less pronounced than for the Gram-negative organism. As found in *Leishmania*, when antibacterial and hemolytic activities were contrasted, 2−3-fold enhancements in SI were found for some analogues, particularly **4** (against either bacteria, also for *Leishmania* promastigotes), as well as **3** and **6** (for *S. aureus*).

Proteolytic Stability of Trimethylated Analogues. As trimethylation protects the Lys residue from proteolysis by trypsin-like enzymes, it was expected that the Lys(Me_3)-substituted analogues would be somewhat more resistant to proteolysis than parent peptide CA(1−7)M(2−9). The time-course of trypsin digests of mono-, disubstituted, and fully substituted analogues of **1** was monitored by LC-MS. As expected, the pertrimethylated analogue **11** was quite impervious to proteolysis, with no appreciable decay throughout the full period of incubation (60 min). Conversely, the parent peptide **1** was 64% degraded after 1 min digestion, with the Lys^6-Lys^7 peptide bond shown as the most vulnerable (De la Torre, manuscript in preparation). Among the monotrimethylated analogues, **4** was particularly resistant (29% degraded at 1 min, 2.2-fold higher proteolytic stability than **1**), arguably because the highly labile Lys^6-Lys^7 bond was protected by trimethylation at Lys^6. Other monotrimethylated analogues (e.g., **5**, **6**) were about 50% degraded after 1 min. On the other hand, analogues **8**, **9**, and **10**, representative of bis-trimethylation, were degraded 20%, 25%, and 19%, respectively, after 1 min. At the 5 min time point, all peptides (except **11**) were largely or totally degraded.

NMR Structural Analysis of Representative Analogues. Further insights into the influence of Lys trimetylation on the structure of CA-M peptides were obtained by NMR analysis of mono- and fully trimethylated analogues **5** and **11**, respectively, in comparison with lead peptide **1**. Resonance assignments were derived from the COSY/TOCSY and NOESY spectra according to the sequential assignment methodology[45] and using the CARA software[46] (see Tables ST1−ST3, Supporting Information).

For all three peptides, ^{1}H NMR spectra in water showed small chemical shift dispersion in the amide region, indicating a predominance of flexible, nonordered structures in fast exchange on the chemical shift NMR time scale. Besides, the two-dimensional NOESY spectra did not contain medium- or long-range NOEs characteristic of any defined and stable conformation. In the presence of 30% (v/v) TFE, however, both chemical shifts and NOE connectivities clearly revealed that stable secondary structures had been induced. First, upfield shifts in the α-protons, characteristic of α-helical structure, were observed for all three peptides. Comparison with the random coil values in the chemical shift index (CSI)[47] (Figure SF1, Supporting Information) showed for most residues deviations strongly indicative of predominantly helical conformation, with the CA less structured than the M segment. The pattern of chemical shift deviations suggested similar conformations for all peptides. In Figure S2 (Supporting Information), a comparison between the αCH chemical shifts of analogues **1**, **5**, and **11** and equivalent residues in the reported NMR data for CA[48] and M[49] suggests relatively less stable helix patterns for all three hybrids, either trimethylated (**5**, **11**) or not (**1**).

Analysis of NOE cross-peak patterns revealed similarities among **1** and its two analogues, such as almost continuous stretches of $d_{NN(i,\,i+1)}$ and $d_{\alpha HN(i,\,i+3)}$ connectivities. A series of strong, helix-specific $d_{\alpha HN(i,i+4)}$-type NOE crosspeaks were also detected for all three peptides. CYANA structure calculations[50] using interproton distance restraints determined from the NOE intensities, plus nonambiguous coupling constants ($^3J_{NH\alpha}$) as angular restraints, allowed proposal of 3D structures for all three peptides. In each case, the 20 best low-energy conformers, all with residues located only in the "most favored" and "allowed" regions of the Ramachandran plot, were chosen for analysis, validated by PROCHECK,[51] and are shown as superimposed representative structures in Figure 4. Inspection of these and previous data suggests that trimethylation induces minimal, nondrastic modifications in secondary structure. Though subtle, these changes may nonetheless suffice to modulate peptide−membrane interaction by increasing flexibility, particularly in the CA region.

Discussion

The biological relevance of Lys methylation has received increasing attention since the discovery of its role as epigenetic modulator of the transcriptional state of chromatin, as well as regulator of the activity of transcriptional factors.[52−54] In these instances, Lys methylation is subtly and tightly regulated, i.e., the biological response appears to rely on the creation of a new specific recognition motif, or on the competition with other Lys modifications,[55] but not strictly on changes in the physicochemical parameters of the Lys side chain. When Lys(Me_3) is incorporated onto AMPs, selectivity of action depends on the initial recognition between a cationic

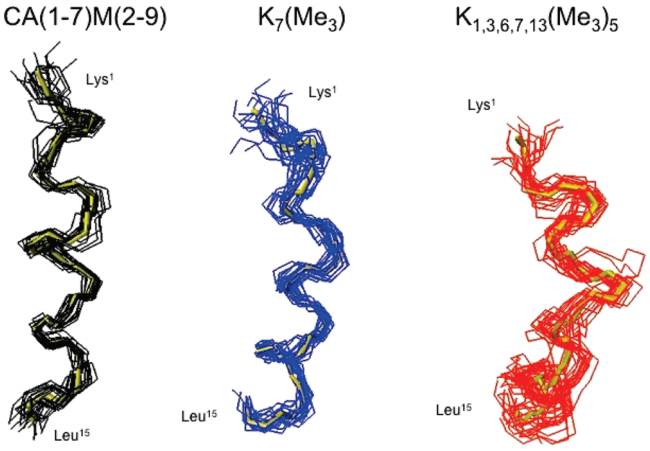

Figure 4. Superimposition of the 20 lowest energy conformers of peptides CA(1−7)M(2−9) (**1**), $K_7(Me_3)$ (**5**) and $K_{1,3,6,7,13}(Me_3)_5$ (**11**). Structures are superimposed over the backbone N, Cα, and C′ atoms of residues 1 through 15.

peptide and the anionic external leaflet of the pathogen membrane, a scenario with much looser specificity requirements.

Prior to the crucial peptide−membrane interaction, the amount of available peptide is controlled by the pathogen's own proteolytic enzymes and/or by peptidases present in the biological fluids that substantially impair the efficacy of the peptide.[56−58] In line with observations on other peptides,[25] in the present case the introduction of one or two Lys(Me_3) residues resulted in 2−3-fold increases in proteolytic resistance, particularly for replacements at Lys[6], the most protease-sensitive position in lead peptide **1**. While this enhanced protease stability cannot be unequivocally used to decode the antimicrobial activity data (Tables 2 and 3), it contributes to the overall performance of the analogues and may be of further relevance in vivo, where the peptide is in prolonged contact with potent degradation systems such as, e.g., leishmaniolysin, a metalloprotease involved in *Leishmania* resistance against AMPs,[59] or other proteases from biological fluids.

Assuming protease resistance to be a coadjuvant though not a decisive factor for the increased SIs of most trimethylated analogues, a more appropriate explanation should look into how the structural changes brought about by trimethylation influence interaction of AMPs with their final target. For CA-M peptides, ample evidence points to permeation of the plasma membrane as the key step in the lethal activity.[37,44,60,61] Here, using *Leishmania* as a model microorganism, membrane permeation has been conclusively linked to peptide killing activity on several counts: (1) trimethylated analogues permeabilize the parasite plasma membrane as assessed by the fast Sytox Green uptake after peptide addition, (2) permeation is also consistent with the fast and severe depletion of intracellular ATP observed upon peptide addition and inducing a lethal bioenergetic collapse, (3) early damage (i.e., at 4 h) to the parasite is in most cases irreversible, as shown by the IC_{50}/LC_{50} ratios close to 1 for most analogues, ruling out a time-dependent mechanism, (4) electron microscopy, particularly with promastigotes, showed plasma membrane permeation and loss of cytoplasmic material after 4 h incubation with peptide, a typical scenario of membrane-active peptides.[37,39,62−64] Membrane permeation appears in this case to take place in an all-or-none fashion, rather than by steadily increasing damage to the entire parasite population. This is not unusual for AMPs of this type, as shown also in *Leishmania* for magainin analogues,[63] or in artificial membranes for CA-M hybrids[65,66] and their parent structures melittin (M)[60,67] and cecropin A (CA).[68]

Having thus established membrane permeation as the lethal mechanism, it is interesting to discuss whether the process is significantly or not affected by Lys trimethylation. Our experimental data show that it lowers the biological activity against all targets, either protozoan or bacterial or eukaryotic. Activity diminishes upon increasing trimethylation and is totally lost in the pertrimethylated analogue **11**, a situation with parallels in melittin[27] and lactoferricin.[26] However, this decreased antimicrobial activity is offset by an even greater loss in activity against eukaryotic cells (measured as hemolysis), which thus results in improved selectivity, particularly for singly trimethylated analogues (Tables 2 and 3). For the two test bacteria (Table 3), as well as for protozoan *Leishmania* promastigotes (though not for amastigotes, Table 2), trimethylation at the more internal Lys residues (e.g., analogues **4** and **5**) is more effective than at the outer ones.

A straightforward interpretation of this general decay of membrane activity with trimethylation is risky given the structural complexity of external barriers such as the peptidoglycan of Gram-positive and the outer membrane of Gram-negative bacteria, both hampering peptide access to the primary plasma membrane target. Despite these caveats, several factors, not mutually exclusive, can still be considered to be at play: (1) Similar to other AMPs with cationic side chains, the present analogues can use their N^{ε}-trimethyl Lys groups to establish electrostatic interactions with anionic phospholipids, common to all the different types of cells tested. (2) Lysine "snorkeling",[69] a term describing the orientation of Lys ε-amino groups to achieve favorable energetics in a membrane interphase, is also possible for N^{ε}-trimethyl groups. In contrast, (3) hydrogen bonds between Lys ε-amino groups and phospholipid phosphate groups will not exist in the trimethylated derivatives. The relative weight of each of these factors requires further investigations that are outside the scope of the present work.

Another structural property that may be affected by trimethylation is hydrophobicity. In the present case, however, the hypothesis is not quite borne out by experimental data. As seen in Table 1, all analogues, including pertrimethylated **11**, elute slightly faster in RP-HPLC than lead peptide **1**. Although the differences in retention times are modest, they may somehow be related with the general trend of reduced hemolytic potency observed. The fact that erythrocytes are zwitterionic in their outward interface suggests that electrostatic interactions may play a lesser role than hydrophobicity in AMP insertion. If so, the lower hydrophobicity of analogues **2**−**11** could translate in poorer insertion (vs parent peptide **1**) and thus account for the differences in SI.

Finally, another area where Lys trimethylation has a presumable impact is peptide conformation. Adoption of an α-helix upon contact with membranes or membrane-like systems is regarded as a key step in peptide−membrane interaction, in contrast with the often unstructured conformation of peptides in water.[30,70,71] At moderate peptide−lipid ratios, lead peptide **1** localizes parallel to the bilayer at the membrane−water interface, with Lys residues exposed and interacting with phospholipid head groups and hydrophobic residues buried into the hydrophobic matrix.[66,70,71] Replacing Lys by considerably bulkier Lys(Me_3) side chains is bound to have conformational consequences, at least in the vicinity of

the replaced residue. While NMR results for analogues **5** and **11** indicate a predominantly helical geometry, they also suggest slightly different levels of flexibility with respect to **1**. This subtle helix-destabilizing action of the Lys(Me_3) residue affects mostly the CA moiety of the peptide and can be plausibly correlated with the observed biological activities by assuming that a slightly more flexible N-terminal (CA) segment is more detrimental for the hemolytic (i.e., increasing HC_{50}) than for the microbicidal activity of the singly trimethylated analogue **5**. According to this view, hemolysis and antimicrobial activity would be related to the structural/dynamic features of the CA and M regions, respectively. The hypothesis would be further supported by the fact that destabilization of both regions, as in analogue **11**, impairs the interaction with both eukaryotic and bacterial membranes and renders the peptide totally ineffective. In summary, NMR results suggest that Lys trimethylation entails a subtle, gradual (with the number of Lys(Me_3) residues) loss in the helical content and rigidity of the peptide, which may explain, within the current consensus theory of AMP−membrane interaction, the slight decrease in potency of monotrimethylated analogues **2**−**6**, the more substantial reduction observed in the four doubly trimethylated analogues **7**−**10** and, especially, the total loss of activity in the pertrimethylated analogue **11**. A related example of helix distortion bringing about a decrease in hemolytic activity and thus an improved SI is provided by the diasteromeric analogues of α-helical AMPs described by Shai.[72] From a more practical point of view, one can also conclude that AMP N^{ε}-trimethylation offers the possibility of improved activity on bacteria of serious clinical concern such as *S. aureus* and *A. baumannii*.[73]

Conclusions

This work serves as a proof-of-principle of the versatility and potentiality of Lys trimethylation as a strategy for fine-tuning AMP biological activity. Trimethylation can hopefully expand the existing armamentarium of subtle modifications aimed at improving the SI of these peptides by either boosting their antimicrobial activity or, as in the present case, diminishing their toxicity. Furthermore, judicious trimethylation of Lys ε-amino groups decreases susceptibility to proteases in biological fluids and/or target pathogens, which results in improved half-lives and thus helps to overcome one of the major hurdles for AMP druggability.

Experimental Section

Peptide Synthesis and Characterization. Fmoc-protected amino acids were obtained from Senn Chemicals (Dielsdorf, Switzerland). Fmoc-Lys(Me_3)-OH was from Iris Biotech (Marktredwitz, Germany). Fmoc-Rink-amide (MBHA) resin was from Novabiochem (Laüfelfingen, Switzerland), and 2-(1*H*-benzotriazol-1-yl)-1,1,3,3-tetramethyluronium hexafluorophosphate (HBTU) and *N*-hydroxybenzotriazole (HOBt) from Matrix Innovation (Montreal, Canada). HPLC-grade acetonitrile (ACN), and peptide synthesis-grade *N*,*N*-dimethylformamide (DMF), *N*,*N*-diisopropylethylamine (DIEA), and trifluoroacetic acid (TFA) were from SDS (Peypin, France).

Solid phase peptide synthesis was done by Fmoc-based chemistry on Fmoc-Rink-amide (MBHA) resin (0.1 mmol) in a model 433 synthesizer (Applied Biosystems, Foster City, CA) running FastMoc protocols. Couplings used 8-fold molar excess each of Fmoc-amino acid, HBTU and HOBt, and 16-fold molar excess of DIEA. Side chains of Lys and Trp residues were protected with the Boc group. Lys(Me_3) was incorporated at the specified positions using the same synthetic file than for Lys. After chain assembly, full deprotection and cleavage was carried out with TFA−water−triisopropylsilane (95:2.5:2.5 v/v, 90 min, rt). Peptides were isolated by precipitation with cold diethyl ether and separated by centrifugation, dissolved in 0.1 M acetic acid and lyophilized. LC-MS was performed in a LC-MS 2010EV instrument (Shimadzu) fitted with a Jupiter C18 column (4.6 mm × 250 mm, 5 μm; Phenomenex) eluted with a 5−95% linear gradient of B into A (A = 0.1% formic acid in water; B = 0.08% formic acid in acetonitrile) over 20 min (see Table 1) at a flow rate of 1 mL/min, with UV detection at 220 nm Preparative HPLC runs were performed on a Luna C18 column (21.2 mm × 250 mm, 10 μm; Phenomenex), using linear gradients of solvent B (0.1% in ACN) into A (0.1% TFA in water), as required, with a flow rate of 25 mL/min. Fractions of high (>95%) HPLC homogeneity and with the expected mass were combined, lyophilized, and used in subsequent experiments.

For proteolytic stability determination, peptides (1 mg/mL in 50 mM NH_4HCO_3) were incubated with trypsin (Promega) at 37 °C in a 1:100 enzyme−peptide ratio. Incubation was terminated by acetic acid addition. The remaining amount of original peptide was determined by HPLC peak integration (elution conditions as above).

Peptide−Membrane Interaction Studies. Unless otherwise stated, reagents were purchased from Sigma (Madrid, Spain) and Merck (Darmstadt, Germany). Bisoxonol [bis-(1,3-diethylthiobarbituric) trimethine oxonol], Sytox Green, and DMNPE-luciferin [1-(4,5-dimethoxy-2-nitrophenyl)-D-luciferin ethyl ester] were from Invitrogen (Barcelona, Spain). Fluorescence and luminescence measurements were recorded in a Polarstar Galaxy microplate reader (BMG Labotechnologies, Germany), fitted with the corresponding optical setting, unless otherwise stated.

Determination of Antimicrobial Activities. *Staphylococcus aureus* strain CECT 240 (kindly provided by the Microbiology Department, University of Granada, Spain) was used to test the bactericidal effect on Gram-positive bacteria. The activity on Gram-negatives was assayed on the opportunistic bacteria *Acinetobacter baumannii* (ATCC 19606). Bacteria were maintained as frozen stocks in order to minimize variations during continuous liquid growth, thawed before the experiment, and grown in Mueller-Hinton II broth (MHB), cation-adjusted (Becton-Dickinson, Cockeysville, MD) at 37 °C. Bactericidal activities were assayed in solution, as described.[74] Briefly, bacteria were collected in exponential growth phase, washed twice with phosphate buffered saline, and resuspended at 1×10^6 CFU/mL in fresh MHB. Aliquots of this suspension were transferred into 96-microwell plates (50 μL/well), and the same volume of a peptide solution at 2 × final concentration in MHB was added to each well. Bacteria were allowed to proliferate overnight at 37 °C, and growth was assessed by turbidimetry at 600 nm in a model 680 microplate reader (Bio-Rad Laboratories, Hercules. CA). Measurements were made by triplicate, and experiments were repeated at least twice.

To assess leishmanicidal activity, protocols previously developed in our laboratory were used.[39,44] Briefly, the *L. donovani* promastigote strain MHOM/SD/00/1S-2D, or the *L. pifanoi* axenic amastigote strain (MHOM/VE/60/Ltrod) were grown in their respective growth media at 26 or 32 °C, respectively. Parasites were harvested at the late exponential growth phase, washed twice in Hank's (136 mM NaCl, 4.2 mM Na_2HPO_4, 4.4 mM KH_2PO_4, 5.4 mM KCl, 4.1 mM $NaHCO_3$, pH 7.2), supplemented with 20 mM D-glucose (Hank's + Glc), resuspended in the same medium (2×10^7 parasites/mL), aliquoted into a 96-microwell plate (120 μL/well final volume), and then treated with peptide. Standard incubation conditions were 4 h at 26 or 32 °C for promastigotes and amastigotes, respectively. After peptide incubation, a 20 μL aliquot was transferred from each well into its respective complete medium and incubated for 72 h at 26 °C or 96 h at 32 °C to allow proliferation of the surviving promastigotes or amastigotes, respectively.

Growth was assessed by incubation of parasites with 0.5 mg/mL of MTT for 2 h at their respective temperature, and final solubilization of the resulting formazan with 5% SDS, which was quantitated spectrophotometrically in a 680 Bio-Rad microplate ELISA reader equipped with a 600 nm filter. For short-time effects, immediately after the 4 h incubation with peptide, a 90 μL aliquot of the parasite suspension was transferred into a 96-microwell plate, an equal volume of MTT (1 mg/mL) added, and incubation continued for an additional 2 h followed by quantitation as above. All experiments were performed by triplicate and repeated at least twice. To illustrate short- and long-term leishmanicidal activity, the IC_{50} and LC_{50} parameters were used (see Abbreviations).

Electron Microscopy. *L. donovani* promastigotes were incubated with peptides under standard conditions, except for a scale up of the incubation volume to 800 μL. Parasites were collected by centrifugation, washed twice with 1 mL of PBS, fixed in 5% (w/v) glutaraldehyde in the same medium, and included with 2.5% (w/v) OsO_4 for 1 h. Next, the cells were gradually dehydrated in ethanol [30, 50, 70, 90, and 100% (v/v); 30 min each], included with propylene oxide (1 h), embedded in Epon 812 resin, and observed in a Jeol-1230 electron microscope.[63]

Real Time Monitoring of in Vivo Changes in Intracellular Levels of ATP in *L. donovani* Promastigotes. A previously described protocol[63] was followed. Briefly, *L. donovani* promastigotes of the 3Luc strain, expressing a cytoplasmic form of luciferase, were resuspended at 2×10^7 promastigotes/mL in Hanks + Glc and incubated at 25 °C with the membrane-permeant luciferase substrate DMNEP-luciferin at 25 μM. When luminescence reached a plateau, peptide was added ($t = 0$) and the ensuing decay in luminescence was monitored in a BMG Polarstar Galaxy microwell reader (Öffenburg, Germany) equipped with luminescence setting. Luminescence data were referred to the percentage of luminescence of the corresponding untreated promastigotes. In vitro inhibition of *Photinus pyralis* luciferase (EC 1.13.12.7) by the peptides was tested with purified enzyme (Roche Applied Sciences, Madrid, Spain) as described.[39]

Hemolysis Assay. The release of hemoglobin from sheep erythrocytes was measured as described.[75] Washed erythrocytes were resuspended in Hank's medium at 2×10^7 cells/mL. Then 100 μL aliquots of this suspension were incubated in 1.5 mL Eppendorf tubes with the peptides (4 h, 37 °C). After centrifugation (14000 rpm, 5 min, 4 °C), 80 μL aliquots of the supernatant were transferred into a 96-well culture microplate and hemoglobin was measured at 550 nm in a Bio-Rad 680 microplate reader. Full lysis was taken as that caused by incubation with 0.1% Triton X-100 (TX-100). HC_{50}, defined as the peptide concentration causing 50% hemoglobin release relative to that obtained with TX-100, was calculated using SigmaPlot v. 11.0. The selectivity index (SI) was defined as the ratio between HC_{50} and LC_{50} (for *Leishmania*) or between HC_{50} and MIC_{50} (for bacteria).

Plasma Membrane Permeation. The loss of *Leishmania* plasma membrane potential was monitored by the increase in fluorescence of the potential-sensitive, anionic dye bisoxonol, upon its insertion into the depolarized parasite membrane. The above standard assay conditions were maintained except for inclusion of 0.2 μM bisoxonol in the incubation medium. Maximal depolarization was defined as that achieved by peptide CA(1−8)M(1−18) at 3.0 μM.[39]

In complementary experiments, the production of larger lesions in the parasite plasma membrane by the peptides was assessed by access of the membrane-impermeable vital dye Sytox Green to the cytoplasm. The above standard assay conditions were maintained except for inclusion of 1 μM final concentration of the probe in the incubation medium. Fluorescence changes were monitored at $\lambda_{ex} = 485$ nm and $\lambda_{em} = 520$ nm. Maximal permeation was defined as that achieved by 0.1% Triton X-100. Sytox Green incorporation into individual parasite cells was assessed by cytofluorometry under the same conditions used above for bulk dye entrance, using a Coulter XL EPICS cytofluorometer.

NMR Spectroscopy. Samples for NMR experiments were dissolved in PBS buffer (pH 6.3) or in TFE-containing aqueous solution (30% v/v trifluoroethanol-d_3, Cambridge Isotope Laboratories) to make a final peptide concentration of ca. 3 mM. Spectra were recorded at 298K on a Bruker DRX-500 spectrometer (^{1}H frequency of 500 MHz) using a 5 mm triple-resonance *Z* gradient probe and processed using XWIN-NMR software (Bruker). The transmitter frequency was set on the HDO/H_2O signal, and the TSP resonance was used as chemical shift reference (δ TSP = 0 ppm). One-dimensional (1D) and two-dimensional (2D) spectra were acquired by standard pulse sequences using WATERGATE-based solvent suppression sequences. Total correlation spectroscopy (TOCSY), and nuclear Overhauser effect spectroscopy (NOESY), were all collected in the phase-sensitive mode using 512 time-proportional phase increments in t1 for each experiment. The free induction decay in t2 consisted of 2K complex data points over a spectral width of 6009.615 Hz. Usually 4096 × 1024 data points were collected for each block, 96 transients were collected for two-dimensional experiments. The spectral width was 10 ppm, and the relaxation delays were set to 1.5 and 2 s in the TOCSY and NOESY experiments, respectively. TOCSY spectra were recorded using the MLEV-17 pulse sequence with mixing times (spin-lock) of 65−80 ms. NOESY experiments were acquired with mixing time of 150−200 ms to avoid any possible contribution from spin diffusion. The NH−CαH scalar couplings were obtained from high-resolution ^{1}H monodimensional spectra. The experimental data were acquired and processed using the TopSpin program on a PC station. The data matrices were multiplied by a qsine function in both dimensions and then zero-filled to 1024 data points in F1 prior to Fourier transformation.

Peak lists for the NOESY spectra recorded with a 0.15−0.2 s mixing time were generated by interactive peak picking using the CARA software.[46] NOESY cross-peak volumes were determined by the automated peak integration routine implemented in CARA. Three-dimensional structures were determined by the standard protocol of the CYANA program (version 2.1),[50] using seven cycles of combined automated NOESY assignment and structure calculations followed by a final structure calculation. Since the Lys(Me_3) residue is not included in the standard CYANA libraries, it was built using the MOLMOL[76] program, also used to visualize the three-dimensional structures. For each CYANA cycle, 1000 randomized conformers and the standard simulated annealing schedule were used. The 20 conformers with the lowest final score were retained for analysis and passed on to the next cycle. Weak restraints on ψ/ψ torsion-angle pairs and on side-chain torsion angles between tetrahedral carbon atoms were applied temporarily during the high-temperature and cooling phases of the simulated annealing schedule in order to favor the permitted regions of the Ramachandran plot and staggered rotamer positions, respectively. The list of upper-distance bonds for the final structural calculation consists of unambiguously assigned upper-distance bonds and does not require the possible swapping of diastereotopic pairs. Next, the 20 conformers with the lowest final CYANA target function values were subjected to restrained energy-minimization in a water shell using the AMBER 8.0 program.[77] The protein was immersed in a shell of water molecules created using the TIP3P model, with a thickness of 10 Å (1 Å = 0.1 nm). The number of additional water molecules oscillated between 2081 and 2991 over the 20 conformers of the three peptides. The restrained energy minimization was performed in three stages. In the first stage, only the water molecules were optimized. Subsequently, the peptide alone was relaxed, maintaining the water molecules fixed, and, finally, the whole system was minimized. In the last stage, a maximum of 1500 steps of restrained energy minimization and a combination of the steepest descent and conjugate gradient algorithms were applied using, in addition to the force field of Cornell et al.,[78] a parabolic or linear penalty function for the NOE upper distance bonds and torsion-angle restraints.

The force constants were chosen such that restraint violations of 0.1 Å and torsion violations of 1° contributed by 0.84 kJ/mol (0.2 kcal/mol) to the potential energy. The resulting 20 energy-minimized conformers represent the solution structure of CA-M and derivatives.

Root-mean-square deviation (rmsd) values were calculated using CYANA for superpositions of the backbone N, Cα, and C′ atoms; the heavy atoms over the whole protein, or over its structured regions. To obtain the rmsd of a structure represented by a bundle of conformers, all conformers were superimposed upon the first one and the average of the rmsd values between the individual conformers and their average coordinates was calculated. Conformational energies were calculated using AMBER 8.0 and applying the force field of Cornell et al.[78]

The statistics regarding the quality and precision of the 20 energy minimized conformers that represent the solution structure of CA-M and derivatives are summarized in Supporting Information Table S4. The quality of the structures was also reflected by the presence of 59.4−87.1% of the (ψ/ψ) backbone torsion-angle pairs in the most favored regions, 12.9−49.6% of which were found within the regions additionally permitted by the Ramachandran plot, according to PROCHECK[51] conventions.

Acknowledgment. This work was supported by the European Union (HEALTH-2007-223414, *Leishdrug*, to L.R. and D.A.), the Spanish Ministry of Science and Innovation (PET2006-0139 to D.A. and L.R., CTQ2009-0856 to J.J.B., BIO2005-07592-CO2-02 and BIO200804487-CO3-02 to D.A.), Fondo de Investigaciones Sanitarias (PI061125, PS09-01928, and RD 06/0021/0006 to L.R., PI040885 to D.A.), and by the regional governments of Madrid (S-BIO-0260/2006 to L.R., BIPPED to J.J.B.) and Catalonia (SGR2005-00494). D.D. is a recipient of a Ramón y Cajal contract from the Spanish Ministry of Science and Innovation.

Supporting Information Available: NMR data and details on structure calculations. This material is available free of charge via the Internet at http://pubs.acs.org.

References

(1) Jenssen, H.; Hamill, P.; Hancock, R. E. W. Peptide antimicrobial agents. *Clin. Microbiol. Rev.* **2006**, *19*, 491–511.
(2) Lievin-Le Moal, V.; Servin, A. L. The front line of enteric host defense against unwelcome intrusion of harmful microorganisms: mucins, antimicrobial peptides, and microbiota. *Clin. Microbiol. Rev.* **2006**, *19*, 315–337.
(3) Matsuzaki, K. Control of cell selectivity of antimicrobial peptides. *Biochim. Biophys. Acta* **2009**, *1788*, 1687–1692.
(4) Melo, M. N.; Ferre, R.; Castanho, M. A. Antimicrobial peptides: linking partition, activity and high membrane-bound concentrations. *Nat. Rev. Microbiol.* **2009**, *7*, 245–250.
(5) Nizet, V. Antimicrobial peptide resistance mechanisms of human bacterial pathogens. *Curr. Issues Mol. Biol.* **2006**, *8*, 11–26.
(6) Pachon, J.; Vila, J. Treatment of multiresistant *Acinetobacter baumannii* infections. *Curr. Opin. Invest. Drugs* **2009**, *10*, 150–156.
(7) Lai, Y.; Gallo, R. L. AMPed up immunity: how antimicrobial peptides have multiple roles in immune defense. *Trends Immunol.* **2009**, *30*, 131–141.
(8) Mookherjee, N.; Rehaume, L. M.; Hancock, R. E. Cathelicidins and functional analogues as antisepsis molecules. *Expert Opin. Ther. Targets* **2007**, *11*, 993–1004.
(9) Zelezetsky, I.; Tossi, A. Alpha-helical antimicrobial peptides—using a sequence template to guide structure−activity relationship studies. *Biochim. Biophys. Acta* **2006**, *1758*, 1436–1449.
(10) Giuliani, A.; Pirri, G.; Bozzi, A.; Di Giulio, A.; Aschi, M.; Rinaldi, A. C. Antimicrobial peptides: natural templates for synthetic membrane-active compounds. *Cell. Mol. Life Sci.* **2008**, *65*, 2450–2460.
(11) Sitaram, N. Antimicrobial peptides with unusual amino acid compositions and unusual structures. *Curr. Med. Chem.* **2006**, *13*, 679–696.
(12) Kutchukian, P. S.; Yang, J. S.; Verdine, G. L.; Shakhnovich, E. I. All-atom model for stabilization of alpha-helical structure in peptides by hydrocarbon staples. *J. Am. Chem. Soc.* **2009**, *131*, 4622–4627.
(13) Smith, B. C.; Denu, J. M. Chemical mechanisms of histone lysine and arginine modifications. *Biochim. Biophys. Acta* **2009**, *1789*, 45–57.
(14) Cedar, H.; Bergman, Y. Linking DNA methylation and histone modification: patterns and paradigms. *Nat. Rev. Genet.* **2009**, *10*, 295–304.
(15) Fingerman, I. M.; Du, H. N.; Briggs, S. D. Controlling histone methylation via *trans*-histone pathways. *Epigenetics* **2008**, *3*, 237–242.
(16) Vaissiere, T.; Sawan, C.; Herceg, Z. Epigenetic interplay between histone modifications and DNA methylation in gene silencing. *Mutat. Res.* **2008**, *659*, 40–48.
(17) Vaillant, I.; Paszkowski, J. Role of histone and DNA methylation in gene regulation. *Curr. Opin. Plant Biol.* **2007**, *10*, 528–533.
(18) Cho, J. H.; Sung, B. H.; Kim, S. C. Buforins: Histone H2A-derived antimicrobial peptides from toad stomach. *Biochim. Biophys. Acta* **2009**, *1788*, 1564–1569.
(19) Koo, Y. S.; Kim, J. M.; Park, I. Y.; Yu, B. J.; Jang, S. A.; Kim, K. S.; Park, C. B.; Cho, J. H.; Kim, S. C. Structure−activity relations of parasin I, a histone H2A-derived antimicrobial peptide. *Peptides* **2008**, *29*, 1102–1108.
(20) Birkemo, G. A.; Luders, T.; Andersen, O.; Nes, I. F.; Nissen-Meyer, J. Hipposin, a histone-derived antimicrobial peptide in Atlantic halibut (*Hippoglossus hippoglossus* L.). *Biochim. Biophys. Acta* **2003**, *1646*, 207–215.
(21) Parseghian, M. H.; Luhrs, K. A. Beyond the walls of the nucleus: the role of histones in cellular signaling and innate immunity. *Biochem. Cell Biol.* **2006**, *84*, 589–604.
(22) Kawasaki, H.; Iwamuro, S. Potential roles of histones in host defense as antimicrobial agents. *Infect. Dis. Drug Targets* **2008**, *8*, 195–205.
(23) Wartha, F.; Beiter, K.; Normark, S.; Henriques-Normark, B. Neutrophil extracellular traps: casting the NET over pathogenesis. *Curr. Opin. Microbiol.* **2007**, *10*, 52–56.
(24) Fernandes, J. M.; Saint, N.; Kemp, G. D.; Smith, V. J. Oncorhyncin III: a potent antimicrobial peptide derived from the non-histone chromosomal protein H6 of rainbow trout, Oncorhynchus mykiss. *Biochem J.* **2003**, *373*, 621–628.
(25) Na, D. H.; Faraj, J.; Capan, Y.; Leung, K. P.; DeLuca, P. P. Stability of antimicrobial decapeptide (KSL) and its analogues for delivery in the oral cavity. *Pharm. Res.* **2007**, *24*, 1544–1550.
(26) Haug, B. E.; Strom, M. B.; Svendsen, J. S. The medicinal chemistry of short lactoferricin-based antibacterial peptides. *Curr. Med. Chem.* **2007**, *14*, 1–18.
(27) Ramalingam, K.; Bello, J. Effect of permethylation on the haemolytic activity of melittin. *Biochem. J.* **1992**, *284* (Pt 3), 663–665.
(28) Merrifield, R. B.; Merrifield, E. L.; Juvvadi, P.; Andreu, D.; Boman, H. G. Design and synthesis of antimicrobial peptides. *Ciba Found. Symp.* **1994**, *186*, 5−20; discussion 20−6.
(29) Rivas, L.; Andreu, D. Cecropin−melittin hybrid peptides as versatile templates in the development of membrane active antibiotics agents. In *Pore-Forming Peptides and Protein Toxins*; Menestrina, G.; Dalla Serra, M., Eds.; Harwood Academic Publishers: Reading, Berkshire, UK, 2003; pp 215−219.
(30) Andreu, D.; Ubach, J.; Boman, A.; Wahlin, B.; Wade, D.; Merrifield, R. B.; Boman, H. G. Shortened cecropin A-melittin hybrids. Significant size reduction retains potent antibiotic activity. *FEBS Lett.* **1992**, *296*, 190–194.
(31) Boman, H. G.; Wade, D.; Boman, I. A.; Wahlin, B.; Merrifield, R. B. Antibacterial and antimalarial properties of peptides that are cecropin−melittin hybrids. *FEBS Lett.* **1989**, *259*, 103–106.
(32) Scott, M. G.; Gold, M. R.; Hancock, R. E. Interaction of cationic peptides with lipoteichoic acid and gram-positive bacteria. *Infect. Immun.* **1999**, *67*, 6445–6453.
(33) Friedrich, C.; Scott, M. G.; Karunaratne, N.; Yan, H.; Hancock, R. E. Salt-resistant alpha-helical cationic antimicrobial peptides. *Antimicrob. Agents Chemother.* **1999**, *43*, 1542–1548.
(34) Piers, K. L.; Brown, M. H.; Hancock, R. E. Improvement of outer membrane-permeabilizing and lipopolysaccharide-binding activities of an antimicrobial cationic peptide by C-terminal modification. *Antimicrob. Agents Chemother.* **1994**, *38*, 2311–2316.
(35) Cavallarin, L.; Andreu, D.; San Segundo, B. Cecropin A-derived peptides are potent inhibitors of fungal plant pathogens. *Mol. Plant−Microbe Interact.* **1998**, *11*, 218–227.
(36) Yevtushenko, D. P.; Romero, R.; Forward, B. S.; Hancock, R. E.; Kay, W. W.; Misra, S. Pathogen-induced expression of a cecropin A-melittin antimicrobial peptide gene confers antifungal resistance in transgenic tobacco. *J. Exp. Bot.* **2005**, *56*, 1685–1695.
(37) Diaz-Achirica, P.; Ubach, J.; Guinea, A.; Andreu, D.; Rivas, L. The plasma membrane of *Leishmania donovani* promastigotes is the

main target for CA(1−8)M(1−18), a synthetic cecropin A-melittin hybrid peptide. *Biochem. J.* **1998**, *330* (Pt 1), 453–460.
(38) Haines, L. R.; Hancock, R. E.; Pearson, T. W. Cationic antimicrobial peptide killing of African trypanosomes and *Sodalis glossinidius*, a bacterial symbiont of the insect vector of sleeping sickness. *Vector Borne Zoonotic Dis.* **2003**, *3*, 175–186.
(39) Luque-Ortega, J. R.; Saugar, J. M.; Chiva, C.; Andreu, D.; Rivas, L. Identification of new leishmanicidal peptide lead structures by automated real-time monitoring of changes in intracellular ATP. *Biochem. J.* **2003**, *375*, 221–230.
(40) Alberola, J.; Rodriguez, A.; Francino, O.; Roura, X.; Rivas, L.; Andreu, D. Safety and efficacy of antimicrobial peptides against naturally acquired leishmaniasis. *Antimicrob. Agents Chemother.* **2004**, *48*, 641–643.
(41) Nos-Barbera, S.; Portoles, M.; Morilla, A.; Ubach, J.; Andreu, D.; Paterson, C. A. Effect of hybrid peptides of cecropin A and melittin in an experimental model of bacterial keratitis. *Cornea* **1997**, *16*, 101–106.
(42) Osusky, M.; Zhou, G.; Osuska, L.; Hancock, R. E.; Kay, W. W.; Misra, S. Transgenic plants expressing cationic peptide chimeras exhibit broad-spectrum resistance to phytopathogens. *Nature Biotechnol.* **2000**, *18*, 1162–1166.
(43) Fields, G. B.; Noble, R. L. Solid phase peptide synthesis utilizing 9-fluorenylmethoxycarbonyl amino acids. *Int. J. Pept. Protein Res.* **1990**, *35*, 161–214.
(44) Chicharro, C.; Granata, C.; Lozano, R.; Andreu, D.; Rivas, L. N-Terminal fatty acid substitution increases the leishmanicidal activity of CA(1−7)M(2−9), a cecropin-melittin hybrid peptide. *Antimicrob. Agents Chemother.* **2001**, *45*, 2441–2449.
(45) Wüthrich, K. *NMR of Proteins and Nucleic Acids*; John Wiley & Sons: New York, 1986.
(46) Keller, R. L. J. *The Computer Aided Resonance Assignment Tutorial*; Cantina Verlag: Goldau, Switzerland, 2004.
(47) Wishart, D. S.; Sykes, B. D.; Richards, F. M. The chemical shift index: a fast and simple method for the assignment of protein secondary structure through NMR spectroscopy. *Biochemistry* **1992**, *31*, 1647–1651.
(48) Holak, T. A.; Engstrom, A.; Kraulis, P. J.; Lindeberg, G.; Bennich, H.; Jones, T. A.; Gronenborn, A. M.; Clore, G. M. The solution conformation of the antibacterial peptide cecropin A: a nuclear magnetic resonance and dynamical simulated annealing study. *Biochemistry* **1988**, *27*, 7620–7629.
(49) Bazzo, R.; Tappin, M. J.; Pastore, A.; Harvey, T. S.; Carver, J. A.; Campbell, I. D. The structure of melittin. A ^{1}H-NMR study in methanol. *Eur. J. Biochem.* **1988**, *173*, 139–146.
(50) Guntert, P. Automated NMR structure calculation with CYANA. *Methods Mol. Biol.* **2004**, *278*, 353–378.
(51) Laskowski, R. A.; MacArthur, M. W.; Moss, D. S.; Thornton, J. M. Procheck: a program to check the stereochemical quality of protein structures. *J. Appl. Crystallogr.* **1993**, *26*, 283–291.
(52) Subramanian, K.; Jia, D.; Kapoor-Vazirani, P.; Powell, D. R.; Collins, R. E.; Sharma, D.; Peng, J.; Cheng, X.; Vertino, P. M. Regulation of estrogen receptor alpha by the SET7 lysine methyltransferase. *Mol. Cell* **2008**, *30*, 336–347.
(53) Scoumanne, A.; Chen, X. Protein methylation: a new mechanism of p53 tumor suppressor regulation. *Histol. Histopathol.* **2008**, *23*, 1143–1149.
(54) Yang, X. D.; Huang, B.; Li, M.; Lamb, A.; Kelleher, N. L.; Chen, L. F. Negative regulation of NF-kappaB action by Set9-mediated lysine methylation of the RelA subunit. *EMBO J.* **2009**, *28*, 1055–1066.
(55) Kurash, J. K.; Lei, H.; Shen, Q.; Marston, W. L.; Granda, B. W.; Fan, H.; Wall, D.; Li, E.; Gaudet, F. Methylation of p53 by Set7/9 mediates p53 acetylation and activity in vivo. *Mol. Cell* **2008**, *29*, 392–400.
(56) Haiko, J.; Suomalainen, M.; Ojala, T.; Lahteenmaki, K.; Korhonen, T. K. Invited review: Breaking barriers—attack on innate immune defences by omptin surface proteases of enterobacterial pathogens. *Innate Immun.* **2009**, *15*, 67–80.
(57) Bachrach, G.; Altman, H.; Kolenbrander, P. E.; Chalmers, N. I.; Gabai-Gutner, M.; Mor, A.; Friedman, M.; Steinberg, D. Resistance of *Porphyromonas gingivalis* ATCC 33277 to direct killing by antimicrobial peptides is protease independent. *Antimicrob. Agents Chemother.* **2008**, *52*, 638–642.
(58) Sieprawska-Lupa, M.; Mydel, P.; Krawczyk, K.; Wojcik, K.; Puklo, M.; Lupa, B.; Suder, P.; Silberring, J.; Reed, M.; Pohl, J.; Shafer, W.; McAleese, F.; Foster, T.; Travis, J.; Potempa, J. Degradation of human antimicrobial peptide LL-37 by *Staphylococcus aureus*-derived proteinases. *Antimicrob. Agents Chemother.* **2004**, *48*, 4673–4679.
(59) Kulkarni, M. M.; McMaster, W. R.; Kamysz, E.; Kamysz, W.; Engman, D. M.; McGwire, B. S. The major surface-metalloprotease of the parasitic protozoan, *Leishmania*, protects against antimicrobial peptide-induced apoptotic killing. *Mol. Microbiol.* **2006**, *62*, 1484–1497.
(60) Ladokhin, A. S.; White, S. H. Folding of amphipathic alpha-helices on membranes: energetics of helix formation by melittin. *J. Mol. Biol.* **1999**, *285*, 1363–1369.
(61) Wieprecht, T.; Beyermann, M.; Seelig, J. Binding of antibacterial magainin peptides to electrically neutral membranes: thermodynamics and structure. *Biochemistry* **1999**, *38*, 10377–10387.
(62) Hernandez, C.; Mor, A.; Dagger, F.; Nicolas, P.; Hernandez, A.; Benedetti, E. L.; Dunia, I. Functional and structural damage in *Leishmania mexicana* exposed to the cationic peptide dermaseptin. *Eur. J. Cell Biol.* **1992**, *59*, 414–424.
(63) Guerrero, E.; Saugar, J. M.; Matsuzaki, K.; Rivas, L. Role of positional hydrophobicity in the leishmanicidal activity of magainin 2. *Antimicrob. Agents Chemother.* **2004**, *48*, 2980–2986.
(64) Granados, E. N.; Bello, J. Interactions of poly (N epsilon, N epsilon, N epsilon, -trimethyllysine) and poly(lysine) with polynucleotides: circular dichroism and A−T sequence selectivity. *Biochemistry* **1981**, *20*, 4761–4765.
(65) Mancheno, J. M.; Onaderra, M.; Martinez del Pozo, A.; Diaz-Achirica, P.; Andreu, D.; Rivas, L.; Gavilanes, J. G. Release of lipid vesicle contents by an antibacterial cecropin A-melittin hybrid peptide. *Biochemistry* **1996**, *35*, 9892–9899.
(66) Bastos, M.; Bai, G.; Gomes, P.; Andreu, D.; Goormaghtigh, E.; Prieto, M. Energetics and partition of two cecropin−melittin hybrid peptides to model membranes of different composition. *Biophys. J.* **2008**, *94*, 2128–2141.
(67) Benachir, T.; Lafleur, M. Study of vesicle leakage induced by melittin. *Biochim. Biophys. Acta* **1995**, *1235*, 452–460.
(68) Gregory, S. M.; Cavenaugh, A.; Journigan, V.; Pokorny, A.; Almeida, P. F. A quantitative model for the all-or-none permeabilization of phospholipid vesicles by the antimicrobial peptide cecropin A. *Biophys. J.* **2008**, *94*, 1667–1680.
(69) Killian, J. A. Synthetic peptides as models for intrinsic membrane proteins. *FEBS Lett.* **2003**, *555*, 134–138.
(70) Abrunhosa, F.; Faria, S.; Gomes, P.; Tomaz, I.; Pessoa, J. C.; Andreu, D.; Bastos, M. Interaction and lipid-induced conformation of two cecropin−melittin hybrid peptides depend on peptide and membrane composition. *J. Phys. Chem. B* **2005**, *109*, 17311–17319.
(71) Bhargava, K.; Feix, J. B. Membrane binding, structure, and localization of cecropin−mellitin hybrid peptides: a site-directed spin-labeling study. *Biophys. J.* **2004**, *86*, 329–336.
(72) Oren, Z.; Hong, J.; Shai, Y. A repertoire of novel antibacterial diastereomeric peptides with selective cytolytic activity. *J. Biol. Chem.* **1997**, *272*, 14643–14649.
(73) Gootz, T. D. The global problem of antibiotic resistance. *Crit. Rev. Immunol.* **2010**, *30*, 79–93.
(74) Saugar, J. M.; Rodriguez-Hernandez, M. J.; de la Torre, B. G.; Pachon-Ibanez, M. E.; Fernandez-Reyes, M.; Andreu, D.; Pachon, J.; Rivas, L. Activity of cecropin A−melittin hybrid peptides against colistin-resistant clinical strains of *Acinetobacter baumannii*: molecular basis for the differential mechanisms of action. *Antimicrob. Agents Chemother.* **2006**, *50*, 1251–1256.
(75) Solanas, C.; de la Torre, B. G.; Fernandez-Reyes, M.; Santiveri, C. M.; Jimenez, M. A.; Rivas, L.; Jimenez, A. I.; Andreu, D.; Cativiela, C. Therapeutic index of gramicidin S is strongly modulated by D-phenylalanine analogues at the beta-turn. *J. Med. Chem.* **2009**, *52*, 664–674.
(76) Koradi, R.; Billeter, M.; Wuthrich, K. MOLMOL: a program for display and analysis of macromolecular structures. *J. Mol. Graphics* **1996**, *14* (51−5), 29–32.
(77) Case, D. A.; Darden, T. E.; Cheatham III, T. E.; Simmerling, C. L.; Wang, J.; Duke, R. E.; Luo, R.; Merz, K. M.; Wang, B.; Pearlman, D. A.; Crowley, M.; Brozell, S.; Tsui, V.; Gohlke, H.; Mongan, J.; Hornak, V.; Cui, G.; Beroza, P.; Schafmeister, C.; Caldwell, J. W.; Ross, W. S.; Kollman, P. A. *AMBER 8*; University of California: San Francisco, 2004.
(78) Cornell, W. D.; Cieplak, P.; Bayly, C. I.; Gould, I. R.; Merz, K. M.; Ferguson, D. M.; Spellmeyer, D. C.; Fox, T.; Caldwell, J. W.; Kollman, P. A. A Second Generation Force Field for the Simulation of Proteins, Nucleic Acids, and Organic Molecules. *J. Am. Chem. Soc.* **1995**, *117*, 5179–5197.